

Superscattering, Superabsorption, and Nonreciprocity in Nonlinear Antennas

Lin Cheng,^{||} Rasoul Alaei,^{*||} Akbar Safari, Mohammad Karimi, Lei Zhang, and Robert W. BoydCite This: <https://dx.doi.org/10.1021/acsp Photonics.0c01637>

Read Online

ACCESS |



Metrics & More



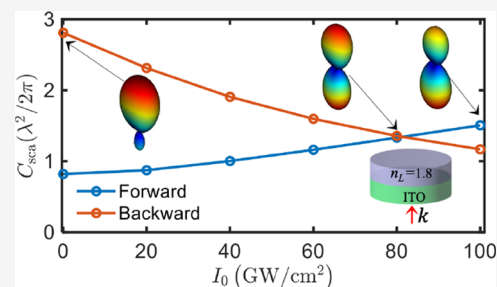
Article Recommendations



Supporting Information

ABSTRACT: We propose tunable nonlinear antennas based on an epsilon-near-zero material with a large optical nonlinearity. We show that the absorption and scattering cross sections of the antennas can be controlled dynamically from a nearly superscatterer to a nearly superabsorber by changing the intensity of the laser. Moreover, we demonstrate that a hybrid nonlinear antenna, composed of epsilon-near-zero and dielectric materials, exhibits nonreciprocal radiation patterns because of broken spatial inversion symmetry and large optical nonlinearity of the epsilon-near-zero material. By changing the intensity of the laser, the radiation pattern of the antenna can be tuned between a bidirectional and a unidirectional emission known as a Huygens source. Our study provides a novel approach toward ultrafast dynamical control of metamaterials, for applications such as beam steering and optical limiting.

KEYWORDS: superscattering, superabsorption, nonreciprocity, epsilon-near-zero (ENZ) materials, Kerker effect, optical antennas



Optical antennas as fundamental building blocks in nanophotonics and metamaterials allow us to manipulate and control optical fields on the nanometer scale.¹ By localizing the energy of a propagating wave, optical antennas provide enhanced control on light–matter interactions for applications such as microscopy² and nonlinear optics.³ Scattering and absorption cross sections are the most important quantities to describe how strong an antenna interacts with the incident light. These cross sections depend on the induced electric and magnetic multipole moments⁴ and can be tailored by engineering either the geometry or the material properties of the optical antennas. Considering their wide applications in photonics, various optical antennas have been proposed to achieve fascinating scattering phenomena, including directional emissions known as the Kerker effects,^{5–7} superscattering,^{8,9} superabsorption,^{10–13} optical cloaking,¹⁴ and nonradiating scattering states.^{15,16}

In order to realize a versatile control of electromagnetic radiation, it is highly desirable to modulate the optical properties of the antennas dynamically. Recently, epsilon-near-zero (ENZ) materials have been shown to exhibit an exceptionally large intensity-dependent refractive index (see Figure 1a).¹⁷ Therefore, ENZ materials provide a new platform to optically tune the response of the material within a subpicosecond time scale.¹⁷ Specifically, negative refraction, tunable metasurfaces, optical switches, tunable cavities, and coherent perfect absorbers have been achieved using indium tin oxide (ITO) and aluminum-doped zinc oxide (AZO) as ENZ materials.^{17–31,31–36}

In this work, we theoretically study the optical response of nonlinear antennas composed of epsilon-near-zero and

dielectric materials. Previously, nonlinear antennas have been realized theoretically and experimentally to enhance nonlinear responses such as second-harmonic and third-harmonic generation.^{37–42} However, the Kerr-type nonlinearity has not been strong enough to significantly modify the scattering response of the antennas at the fundamental wavelength. In our work, the large Kerr-type nonlinearity of the ENZ material plays a crucial role in changing the induced multipole moments and, thus, drastically modifying the scattering, absorption, and extinction cross sections as well as the radiation pattern of the antennas. In particular, we can optically switch the antennas' response from a nearly superscattering to a nearly superabsorbing state. By employing the multipole expansion of the induced intensity-dependent polarization current, we show that the radiation pattern of the antennas can be tuned from a nondirective to a nearly Huygens source by changing the intensity of the laser. In this work, the terms “scatterers” and “antennas” can be used interchangeably.

■ NONLINEAR ANTENNAS BASED ON ENZ MATERIALS

Let us consider a nonlinear antenna made of indium tin oxide (ITO; see the inset of Figure 1b). The antenna is illuminated

Received: October 22, 2020

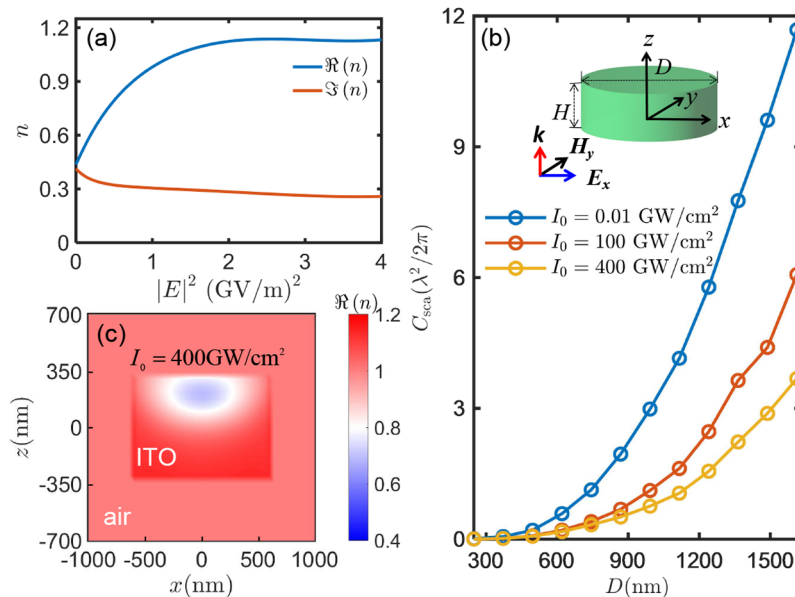


Figure 1. Nonlinear antenna based on epsilon-near-zero (ENZ) material: (a) The real and imaginary parts of the intensity-dependent refractive index of ITO at the ENZ wavelength $\lambda_{\text{ENZ}} = 1240$ nm (see ref 21). (b) Scattering cross section (normalized to $\lambda^2/2\pi$) of the ITO antenna at the ENZ wavelength as a function of the diameter of the antenna D for different intensities. Note that the lowest intensity, that is, $I_0 = 0.01$ GW/cm 2 , corresponds to the linear response of the antenna. Inset shows a schematic of the ITO disk with height H and diameter D . The ITO antenna is illuminated by an x -polarized plane wave propagating in the z direction. (c) The real part of refractive index in the xz -plane (at $y = 0$) at the highest intensity, that is, $I_0 = 400$ GW/cm 2 . We assume that the height of the ITO antenna is $H = D/2$ and the surrounding medium is air.

by an x -polarized time-harmonic plane wave with electric field $\mathbf{E}_{\text{inc}}(t) = (E_0/2)e^{i(kz - \omega t)}\mathbf{e}_x + \text{c.c.}$, where $|k| = 2\pi/\lambda$ is the wavenumber, ω is the angular frequency, E_0 is the amplitude of incident field, and c.c. means complex conjugate. $I_0 = \frac{1}{2}c\epsilon_0|E_0|^2$ is the free-space intensity of the incident plane wave. The intensity-dependent refractive index of ITO is $n_{\text{NL}}(\mathbf{r}, \omega) = \sqrt{\epsilon_{\text{NL}}(\mathbf{r}, \omega)}$, where $\epsilon_{\text{NL}}(\mathbf{r}, \omega)$ is given by^{21,43}

$$\epsilon_{\text{NL}}(\mathbf{r}, \omega) \approx \epsilon_L + \sum_{j=1}^3 c_{2j+i} \chi^{(2j+1)}(\omega) \left| \frac{\mathbf{E}(\mathbf{r}, \omega)}{2} \right|^{2j} \quad (1)$$

and where $\chi^{(3)}(\omega)$, $\chi^{(5)}(\omega)$, and $\chi^{(7)}(\omega)$ are the third-order, fifth-order, and seventh-order nonlinear susceptibilities (see Table 1 in ref 21) of ITO, respectively. $c_3 = 3$, $c_5 = 10$, and $c_7 = 35$ are the degeneracy factors,⁴³ and $\mathbf{E}(\mathbf{r}, \omega)$ is the electric field amplitude inside ITO.

The real part of the permittivity of ITO is zero at $\lambda_{\text{ENZ}} = 1240$ nm, which is called the ENZ wavelength. It has been shown that ITO exhibits a large nonlinear refractive index around its ENZ wavelength.^{17,20,21} Figure 1a plots the real and imaginary parts of the intensity-dependent refractive index of the ITO film at λ_{ENZ} .^{17,21} Note that the change in the real part of the refractive index by intensity is approximately 0.72, which is even larger than the linear refractive index of ITO, which is 0.4. In the following, we incorporate this large nonlinear response of ITO at the ENZ wavelength and perform our simulations using a Maxwell's equations numerical solver combined with an iterative method to solve for an intensity-dependent refractive index inside the antenna.

In order to understand the optical response of the proposed nonlinear antennas, we employ multipole expansion of the induced nonlinear (intensity-dependent) polarization current $\mathbf{J}_{\text{NL}}(\mathbf{r}, \omega) = -i\omega[\epsilon_{\text{NL}}(\mathbf{r}, \omega) - \epsilon_0]\mathbf{E}(\mathbf{r}, \omega)$.^{4,44} Through use of the

induced multipole moments, the total scattering cross section of the nonlinear ITO antenna can be calculated by^{4,44}

$$C_{\text{sca}} = \frac{k^4}{6\pi\epsilon_0^2|E_0|^2} \left[\sum_{\alpha} \left(|p_{\alpha}|^2 + \left| \frac{m_{\alpha}}{c} \right|^2 \right) + \sum_{\alpha, \beta} \left(\left| kQ_{\alpha\beta}^e \right|^2 + \left| \frac{kQ_{\alpha\beta}^m}{c} \right|^2 \right) \right] \quad (2)$$

as a sum of contribution of each multipole moment to the total scattering cross section. $\alpha, \beta = x, y, z$, and p_{α} , m_{α} , $Q_{\alpha\beta}^e$, and $Q_{\alpha\beta}^m$ are the electric dipole (ED), magnetic dipole (MD), electric quadrupole (EQ), and magnetic quadrupole (MQ) moments.

Figure 1b shows the scattering cross section (normalized to $\lambda^2/2\pi$) of the ITO disk as a function of its diameter D for three different intensities. It can be seen that the scattering cross section gradually increases as D increases. At high intensities, for example, $I_0 = 400$ GW/cm 2 , the scattering cross section is approximately 4 \times smaller than the linear response, that is, $I_0 = 0.01$ GW/cm 2 (see Supporting Information). At high intensities, the refractive index of ITO is close to the refractive index of the surrounding medium (air), and thus, scattering becomes smaller than that of low intensities (Figure 1a,c). These results can also be understood in terms of the induced electric and magnetic multipole moments (see Supporting Information for details). In Figure 1c, we plot the real part of the refractive index of the ITO antenna in the xz -plane. The refractive index depends on position \mathbf{r} because of the induced nonuniform electric field distribution inside the antenna, that is, $\mathbf{E}(\mathbf{r})$ (see also eq 1).

Figure 2a shows the total scattering cross section and contributions of the electric and magnetic multipole moments as a function of intensity. Although the contribution of the ED moment is significantly larger than any other modes, the antenna radiates mainly in the forward direction because of the presence of higher order moments (Figure 2a,b). The

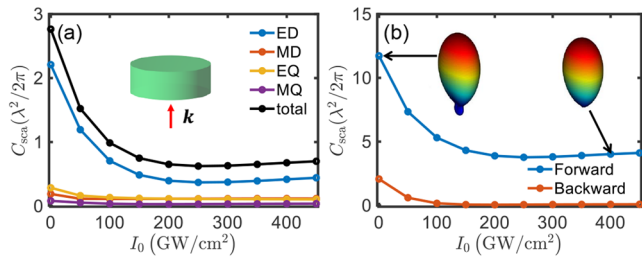


Figure 2. Intensity-dependent response of a nonlinear antenna: (a) Total scattering cross section (normalized to $\lambda^2/2\pi$) and contribution of different electric and magnetic multipole moments as a function of the input intensity for the ITO antenna. Contribution of different multipoles are labeled by ED (electric dipole), MD (magnetic dipole), EQ (electric quadrupole), and MQ (magnetic quadrupole). The geometrical parameters of the ITO antenna are $D = 0.8\lambda_{\text{ENZ}}$ and $H = D/2$. (b) Normalized forward and backward scattering cross sections calculated from eq 3. The insets illustrate normalized far-field radiation patterns of the ITO antenna for low and high intensities.

normalized forward $C_{\text{sca}}^{\text{F}}$ and backward $C_{\text{sca}}^{\text{B}}$ scattering cross sections are plotted in Figure 2b, which are calculated from⁷

$$C_{\text{sca}}^{\text{F/B}} = C_{\text{norm}} \left| p_x \pm \frac{m_y}{c} \mp \frac{ikQ_{xz}^e}{6} - \frac{ikQ_{yz}^m}{6c} \right|^2 \quad (3)$$

where $C_{\text{norm}} = k^4/(4\pi\epsilon_0^2|E_0|^2)$. In eq 3, the forward and backward scattering cross sections are calculated at $\phi_{\text{F/B}} = 0$ and $\theta_{\text{F/B}} = 0, \pi$. Note that the ED (and similarly MQ) moment exhibits in-phase forward and backward scattered electric fields, whereas the MD (and similarly EQ) moment shows out-of-phase fields (see \pm in eq 3). As the intensity of the laser increases, the contribution of different multipoles changes. Consequently, the antenna radiates solely in the forward direction at high intensities, which is clearly evident from the inset of Figure 2b.

■ SUPERABSORPTION AND SUPERSCATTERING IN NONLINEAR ANTENNAS

The maximum scattering cross section (for each multipolar order) of an isotropic nanoparticle with multipolar response is $C_{\text{sca},j}^{\text{max}} = (2j+1)\lambda^2/2\pi$, where j is the order of the multipole; for example, $j = 1, 2,$ and 3 , for dipoles, quadrupoles, and octupoles, respectively.^{8,9,11,13,45,46} For each multipolar order, the maximum scattering occurs at the resonance for a particle with negligible Ohmic losses compared to the radiation loss (this condition is known as overcoupling).^{8,9,11,13,45–48} By engineering subwavelength nanoparticles, it is possible to achieve a much larger scattering cross section compared to a dipolar one, that is, $C_{\text{sca},1}^{\text{max}} = 3\lambda^2/2\pi$. This phenomenon is known as superscattering and is achieved by overlapping resonant frequencies of different multipoles.^{8,9,12,13} It has also been shown that the maximum absorption cross section of a nanoparticle with multipolar response is limited to $C_{\text{abs},j}^{\text{max}} = C_{\text{sca},j}^{\text{max}}/4 = (2j+1)\lambda^2/8\pi$.^{11–13,46} The enhanced absorption can be achieved for particles that operate at critical coupling (i.e., nonradiative or Ohmic loss is equal to the radiation loss) and by aligning the resonance frequencies of different multipoles. This enhanced absorption cross section is known as superabsorption.^{8,9}

Here, we show that scattering and absorption cross sections of an ITO antenna can be tuned between nearly superscattering and nearly superabsorbing states by simply changing

the input laser intensity. Figure 3a,b shows scattering and absorption cross sections of our ITO antenna as a function of

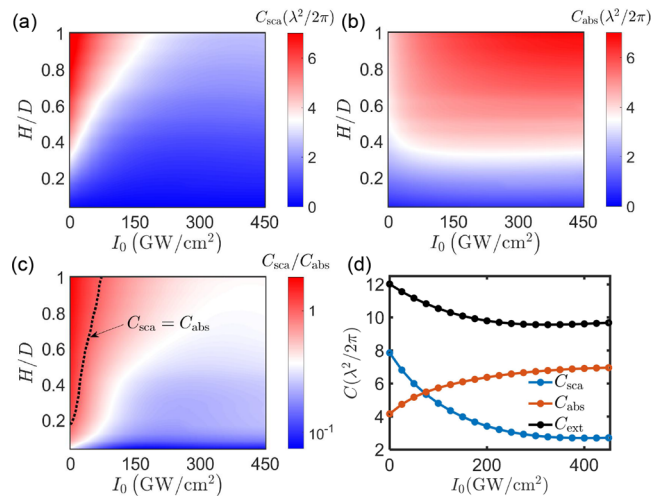


Figure 3. Tunable superabsorption and superscattering based on an ITO antenna: (a) Total scattering cross section C_{sca} (normalized to $\lambda^2/2\pi$) of the ITO antenna (see the inset of Figure 1b) as a function of height-to-diameter ratios, H/D , and the laser intensity I_0 , where the diameter of the antenna $D = 1200$ nm. (b) Same as (a) for the absorption cross section, that is, C_{abs} . (c) The ratio between the scattering and absorption cross sections shown in logarithmic scale. The black dashed line indicates the condition that the scattering and absorption cross sections are equal, that is, $C_{\text{sca}} = C_{\text{abs}}$. (d) Scattering, absorption, and extinction cross sections as functions of intensity I_0 for $H = D = 1200$ nm.

the laser intensity for different height-to-diameter ratios, H/D . For low intensities and $H/D = 1$, the scattering cross section is $C_{\text{sca}} \approx 2.7 \times 3\lambda^2/2\pi$, which is $2.7\times$ larger than the maximum scattering of a dipole. By increasing the laser intensity, the absorption cross section increases and reaches to $C_{\text{abs}} \approx 9.3 \times 3\lambda^2/8\pi$, which is significantly larger than that of a dipolar scatterer. Therefore, the ITO antenna behaves as a super-scatterer at low intensities and as a superabsorber at high intensities. This behavior can be seen clearly from Figure 3d, which plots the scattering, absorption, and extinction cross sections as a function of intensity for $H = D = 1200$ nm. The ratio of the scattering to the absorption cross section is depicted in Figure 3c (the induced electric and magnetic multipole moments of the antenna are shown in Supporting Information). Three distinct coupling regimes are evident: (i) a large scattering cross section compared to absorption, that is, $C_{\text{sca}} > C_{\text{abs}}$, the area to the left of the black dashed line, (ii) scattering is identical to absorption cross section, that is, $C_{\text{sca}} = C_{\text{abs}}$, as indicated by the black dashed line in Figure 3c, and (iii) a large absorption cross section compared to scattering, that is, $C_{\text{abs}} > C_{\text{sca}}$, the area to the right of the black dashed line.

■ HYBRID NONRECIPROCAL NONLINEAR ANTENNAS

Dielectric antennas support strong electric and magnetic responses with large scattering cross sections.^{45,49,50} Thus, to achieve an even greater control on the scattering properties of ITO antennas, one can devise a nonlinear antenna composed of ENZ and lossless dielectric materials. In the following, we consider a hybrid nonlinear antenna made of an ITO and a lossless linear dielectric material with refractive index n_l , as

shown in the inset of Figure 4a. Due to the broken inversion symmetry, the hybrid antenna exhibits magneto–electric coupling or the so-called bianisotropic response.^{51–53}

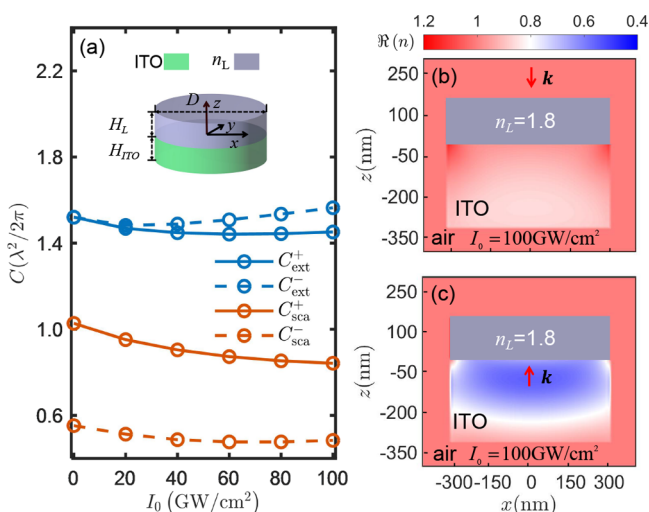


Figure 4. Hybrid nonlinear antenna composed of ITO and a lossless linear dielectric material with refractive index $n_L = 1.8$: (a) Total extinction (C_{ext}^{\pm}) and scattering (C_{sca}^{\pm}) cross sections (normalized to $\lambda^2/2\pi$) of the hybrid antenna as a function of the laser intensity when illuminated by an x -polarized plane wave propagating in two opposite directions, that is, $\mathbf{k} = \pm k_0 \mathbf{e}_z$. Inset shows the schematic of the hybrid nonlinear antenna. (b, c) The real part of refractive index in xz -plane (at $y = 0$) at intensity $I_0 = 100 \text{ GW/cm}^2$ for top ($\mathbf{k} = -k_0 \mathbf{e}_z$) and bottom ($\mathbf{k} = +k_0 \mathbf{e}_z$) illuminations, respectively. The surrounding medium is air. The geometrical parameters of the hybrid nonlinear antenna are $D_{\text{ITO}} = D_L = D = 620 \text{ nm}$, $H_{\text{ITO}} = D_{\text{ITO}}/2$, and $H_L = 150 \text{ nm}$.

According to the optical theorem and the Lorentz reciprocity, the extinction cross section of an arbitrarily shaped antenna made of reciprocal materials is the same for two opposite illumination directions.^{52,54–56} However, the scattering and absorption cross sections of the reciprocal antenna depend on the illumination direction due to absorption (Ohmic) losses which are related to the induced bianisotropic response.^{52,56} In Figure 4a we plot the extinction and scattering cross sections of the hybrid antenna when illuminated from opposite directions ($\mathbf{k} = \pm k_0 \mathbf{e}_z$). In the linear regime (low intensities), the antenna is reciprocal. Therefore, the extinction cross section for top and bottom illuminations are identical, that is, $C_{\text{ext}}^+ = C_{\text{ext}}^-$.^{52,56} However, the scattering (and also the absorption) cross sections of the antenna are different, $C_{\text{sca}}^+ \neq C_{\text{sca}}^-$.

At high laser intensities, the hybrid antenna is nonreciprocal and two conditions to break the Lorentz reciprocity are simultaneously satisfied, that is, the large optical nonlinearity and lack of inversion symmetry.⁵⁷ Thus, as shown in Figure 4a, the extinction cross sections of the antenna are not the same for the two opposite illuminations at high intensities. Figure 4b,c shows the real part of the refractive index in the xz -plane for $I_0 = 100 \text{ GW/cm}^2$ and indicate a position-dependent refractive index. Clearly, the refractive indices are different for opposite illuminations: $n_{\text{NL}}^+(\mathbf{r}) \neq n_{\text{NL}}^-(\mathbf{r})$. The different distribution of the refractive indices (Figure 4b,c) leads to a magneto–electric coupling (see ref 52 for a magneto–electric coupling in a reciprocal antenna). To understand the underlying physics of the asymmetric nonreciprocal response

and magneto–electric coupling, we compute the induced multipole moments using the exact multipole expansion for the opposite illuminations (see Figure 5a,b). The induced

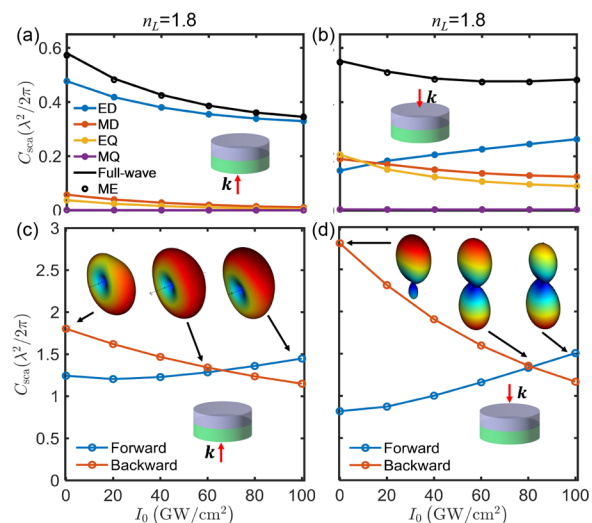


Figure 5. Scattering and radiation patterns of hybrid nonlinear antennas: (a) Total scattering cross section (normalized to $\lambda^2/2\pi$) and contribution of different electric and magnetic multipole moments of the hybrid antenna as a function of the laser intensity for the bottom illumination direction, that is, $\mathbf{k} = +k_0 \mathbf{e}_z$. (c) Normalized forward (blue line) and backward (red line) scattering cross sections calculated from eq 3 for the bottom illumination direction. Insets illustrate far-field radiation patterns of hybrid nonlinear antenna in three intensities for the bottom illumination direction, that is, $\mathbf{k} = +k_0 \mathbf{e}_z$. (b, d) Same as (a) and (c) for the top illumination direction, that is, $\mathbf{k} = -k_0 \mathbf{e}_z$.

multipole moments are significantly different for the top and bottom illuminations which lead to intensity-dependent magneto–electric coupling. Note that the scattering cross sections calculated using full-wave simulation as well as multipole expansion (ME) are in perfect agreement (see the black solid line and circles in Figure 5a,b). Therefore, our proposed nonlinear scatterer can be fully characterized by using the dipole and quadrupole moments.

When the hybrid antenna is illuminated from the bottom, the antenna exhibits mainly an electric dipole (ED) moment, as can be seen in Figure 5a. Therefore, the radiation pattern of hybrid antenna is nearly omnidirectional (see the inset of Figure 5c). The contribution of other multipole moments to the forward and backward cross sections are small compared to the ED moment and thus slightly modify the radiation patterns.

When the hybrid antenna is illuminated from the top, compared to the bottom illumination, different multipole moments contribute to the scattering (compare Figure 5a and b). However, similar to the bottom illumination, the backward (forward) scattering decreases (increases) with the intensity, as shown in Figure 5d. In the linear regime (low intensities), the induced ED, MD, and EQ moments interfere constructively (destructively) in the backward (forward) direction. Consequently, the antenna exhibits a nearly unidirectional radiation pattern with a very small forward scattering (see Figure 5d). At $I_0 \approx 80 \text{ GW/cm}^2$, the forward and backward scattering become identical. In the Supporting Information, we show that a hybrid antenna with $n_L = 3.5$ exhibits a unidirectional radiation

pattern with nearly zero backward scattering. This phenomena is known as the generalized Kerker effect.^{7,58} Large tunability of the induced multipole moments of the hybrid antenna by an intense pump laser allows to control the radiation patterns from a bidirectional to a unidirectional pattern (compare three radiation patterns in the inset of Figure 5d). Therefore, by employing an ultrafast optical pump,¹⁷ the radiation pattern of the hybrid antenna can be switched from a nondirective radiation to a directive one within a subpicosecond time scale. Moreover, the hybrid antenna exhibits nonreciprocal radiation patterns because of nonreciprocal magneto-electric coupling.

In summary, we have theoretically studied nonlinear antennas based on ENZ materials with tunable absorption and scattering cross sections, as well as radiation patterns. We incorporated the extremely large and ultrafast nonlinear response of ENZ materials, in particular, ITO. We showed that while the radiation pattern of a single ITO antenna remains insensitive to the laser intensity, its absorption, scattering, and extinction cross sections can be modulated dynamically. Therefore, the antenna can be tuned between superabsorbing and superscattering states by controlling the intensity of the laser. Furthermore, we proposed a hybrid antenna (composed of ITO and a dielectric material) with a radiation pattern that can be tuned between bidirectional and unidirectional emission under ultrafast optical pumping. Moreover, we found that the hybrid nanoantenna exhibits tunable nonreciprocal radiation patterns when illuminated from opposite directions because of the broken spatial inversion symmetry and large optical nonlinearity of ITO. We explained our findings based on the interference among the induced intensity-dependent electric and magnetic multipole moments. Considering the fast response-time of ITO, a typical 100 fs pulsed laser can be used to achieve the required intensities experimentally.^{17,26} The proposed tunable hybrid antenna with magneto-electric response can be used as a building block to design ultrafast switchable nonreciprocal electric and magnetic mirrors,^{57,59} metalens,⁵⁷ metaabsorbers,^{48,60} metagrating,⁶¹ and photonic topological insulators.⁶² In addition, our work provides a novel approach for designing tunable nanoantennas based on ENZ materials with a large optical nonlinearity.

■ ASSOCIATED CONTENT

SI Supporting Information

The Supporting Information is available free of charge at <https://pubs.acs.org/doi/10.1021/acsphotonics.0c01637>.

We present expressions for the exact induced multipole moments in Cartesian coordinates, the corresponding scattering cross sections, and the intensity-dependent refractive index, and the multipole moments for the superabsorption and superscattering states (PDF)

■ AUTHOR INFORMATION

Corresponding Author

Rasoul Alaei – Department of Physics, University of Ottawa, Ottawa, Ontario K1N 6N5, Canada; orcid.org/0000-0003-2187-4949; Email: rasoul.alaei@gmail.com

Authors

Lin Cheng – Department of Physics, University of Ottawa, Ottawa, Ontario K1N 6N5, Canada; Key Laboratory of Physical Electronics and Devices of Ministry of Education

School of Electronic Science and Engineering, Xi'an Jiaotong University, Xi'an 710049, China

Akbar Safari – Department of Physics, University of Ottawa, Ottawa, Ontario K1N 6N5, Canada

Mohammad Karimi – Department of Physics, University of Ottawa, Ottawa, Ontario K1N 6N5, Canada

Lei Zhang – Key Laboratory of Physical Electronics and Devices of Ministry of Education, School of Electronic Science and Engineering, Xi'an Jiaotong University, Xi'an 710049, China; orcid.org/0000-0002-5113-1786

Robert W. Boyd – Department of Physics, University of Ottawa, Ottawa, Ontario K1N 6N5, Canada; The Institute of Optics, University of Rochester, Rochester, New York 14627, United States; orcid.org/0000-0002-1234-2265

Complete contact information is available at:

<https://pubs.acs.org/10.1021/acsphotonics.0c01637>

Author Contributions

^{||}These authors contributed equally to this work.

Notes

The authors declare no competing financial interest.

■ ACKNOWLEDGMENTS

R.A. acknowledges the support of the Alexander von Humboldt Foundation through the Feodor Lynen Fellowship. L.C. acknowledges the support of China Scholarship Council. L.C., R.A., A.S., M.K., and R.W.B. are grateful to M. Zahirul Alam, Orad Reshef, Boris Braverman, and Jeremy Upham for helpful discussions and acknowledge support through the Natural Sciences and Engineering Research Council of Canada, the Canada Research Chairs program, and the Canada First Research Excellence Fund. R.W.B. also acknowledges support from the U.S. Army Research Office and the U.S. Defense Advanced Research Projects Administration. R.A. would like to thank Orad Reshef for providing data for Figure 1_a.

■ REFERENCES

- (1) Bharadwaj, P.; Deutsch, B.; Novotny, L. Optical antennas. *Adv. Opt. Photonics* **2009**, *1*, 438–483.
- (2) Taylor, R. W.; Sandoghdar, V. *Label-Free Super-Resolution Microscopy*; Springer, 2019; pp 25–65.
- (3) Krasnok, A.; Tymchenko, M.; Alù, A. Nonlinear metasurfaces: a paradigm shift in nonlinear optics. *Mater. Today* **2018**, *21*, 8–21.
- (4) Alaei, R.; Rockstuhl, C.; Fernandez-Corbaton, I. Exact multipolar decompositions with applications in nanophotonics. *Adv. Opt. Mater.* **2019**, *7*, 1800783.
- (5) Kerker, M.; Wang, D.-S.; Giles, C. Electromagnetic scattering by magnetic spheres. *J. Opt. Soc. Am.* **1983**, *73*, 765–767.
- (6) Zambrana-Puyalto, X.; Fernandez-Corbaton, I.; Juan, M.; Vidal, X.; Molina-Terriza, G. Duality symmetry and Kerker conditions. *Opt. Lett.* **2013**, *38*, 1857–1859.
- (7) Alaei, R.; Filter, R.; Lehr, D.; Lederer, F.; Rockstuhl, C. A generalized Kerker condition for highly directive nanoantennas. *Opt. Lett.* **2015**, *40*, 2645–2648.
- (8) Ruan, Z.; Fan, S. Superscattering of light from subwavelength nanostructures. *Phys. Rev. Lett.* **2010**, *105*, No. 013901.
- (9) Ruan, Z.; Fan, S. Design of subwavelength superscattering nanospheres. *Appl. Phys. Lett.* **2011**, *98*, 043101.
- (10) Ng, J.; Chen, H.; Chan, C. T. Metamaterial frequency-selective superabsorber. *Opt. Lett.* **2009**, *34*, 644–646.
- (11) Miroshnichenko, A. E.; Tribelsky, M. I. Ultimate absorption in light scattering by a finite obstacle. *Phys. Rev. Lett.* **2018**, *120*, No. 033902.

- (12) Estakhri, N. M.; Alu, A. Minimum-scattering superabsorbers. *Phys. Rev. B: Condens. Matter Mater. Phys.* **2014**, *89*, 121416.
- (13) Rahimzadegan, A.; Alaei, R.; Fernandez-Corbaton, I.; Rockstuhl, C. Fundamental limits of optical force and torque. *Phys. Rev. B: Condens. Matter Mater. Phys.* **2017**, *95*, No. 035106.
- (14) Alù, A.; Engheta, N. Multifrequency Optical Invisibility Cloak with Layered Plasmonic Shells. *Phys. Rev. Lett.* **2008**, *100*, 113901.
- (15) Devaney, A. J.; Wolf, E. Radiating and Nonradiating Classical Current Distributions and the Fields They Generate. *Phys. Rev. D: Part. Fields* **1973**, *8*, 1044–1047.
- (16) Hsu, C. W.; DeLacy, B. G.; Johnson, S. G.; Joannopoulos, J. D.; Soljacic, M. Theoretical criteria for scattering dark states in nanostructured particles. *Nano Lett.* **2014**, *14*, 2783–2788.
- (17) Alam, M. Z.; De Leon, I.; Boyd, R. W. Large optical nonlinearity of indium tin oxide in its epsilon-near-zero region. *Science* **2016**, *352*, 795–797.
- (18) Argyropoulos, C.; Chen, P.-Y.; D'Aguanno, G.; Engheta, N.; Alù, A. Boosting optical nonlinearities in ϵ -near-zero plasmonic channels. *Phys. Rev. B: Condens. Matter Mater. Phys.* **2012**, *85*, No. 045129.
- (19) Kinsey, N.; DeVault, C.; Kim, J.; Ferrera, M.; Shalaev, V.; Boltasseva, A. Epsilon-near-zero Al-doped ZnO for ultrafast switching at telecom wavelengths. *Optica* **2015**, *2*, 616–622.
- (20) Caspani, L.; Kaipurath, R. P. M.; Clerici, M.; Ferrera, M.; Roger, T.; Kim, J.; Kinsey, N.; Pietrzyk, M.; Di Falco, A.; Shalaev, V. M.; Boltasseva, A.; Faccio, D. Enhanced Nonlinear Refractive Index in ϵ -Near-Zero Materials. *Phys. Rev. Lett.* **2016**, *116*, 233901.
- (21) Reshef, O.; Giese, E.; Alam, M. Z.; De Leon, I.; Upham, J.; Boyd, R. W. Beyond the perturbative description of the nonlinear optical response of low-index materials. *Opt. Lett.* **2017**, *42*, 3225–3228.
- (22) Liberal, I.; Engheta, N. Near-zero refractive index photonics. *Nat. Photonics* **2017**, *11*, 149.
- (23) Clerici, M.; Kinsey, N.; DeVault, C.; Kim, J.; Carnemolla, E. G.; Caspani, L.; Shaltout, A.; Faccio, D.; Shalaev, V.; Boltasseva, A.; Ferrera, M. Controlling hybrid nonlinearities in transparent conducting oxides via two-colour excitation. *Nat. Commun.* **2017**, *8*, 1–7.
- (24) Ferrera, M.; Kinsey, N.; Shaltout, A.; DeVault, C.; Shalaev, V.; Boltasseva, A. Dynamic nanophotonics. *J. Opt. Soc. Am. B* **2017**, *34*, 95–103.
- (25) Liberal, I.; Engheta, N. The rise of near-zero-index technologies. *Science* **2017**, *358*, 1540–1541.
- (26) Alam, M. Z.; Schulz, S. A.; Upham, J.; De Leon, I.; Boyd, R. W. Large optical nonlinearity of nanoantennas coupled to an epsilon-near-zero material. *Nat. Photonics* **2018**, *12*, 79.
- (27) Vezzoli, S.; Bruno, V.; DeVault, C.; Roger, T.; Shalaev, V. M.; Boltasseva, A.; Ferrera, M.; Clerici, M.; Dubietis, A.; Faccio, D. Optical time reversal from time-dependent Epsilon-Near-Zero media. *Phys. Rev. Lett.* **2018**, *120*, No. 043902.
- (28) Kim, J.; Carnemolla, E. G.; DeVault, C.; Shaltout, A. M.; Faccio, D.; Shalaev, V. M.; Kildishev, A. V.; Ferrera, M.; Boltasseva, A. Dynamic control of nanocavities with tunable metal oxides. *Nano Lett.* **2018**, *18*, 740–746.
- (29) Niu, X.; Hu, X.; Chu, S.; Gong, Q. Epsilon-Near-Zero Photonics: A New Platform for Integrated Devices. *Adv. Opt. Mater.* **2018**, *6*, 1701292.
- (30) Reshef, O.; De Leon, I.; Alam, M. Z.; Boyd, R. W. Nonlinear optical effects in epsilon-near-zero media. *Nature Reviews Materials* **2019**, *4*, 535–551.
- (31) Kinsey, N.; DeVault, C.; Boltasseva, A.; Shalaev, V. M. Near-zero-index materials for photonics. *Nature Reviews Materials* **2019**, *4*, 742–760.
- (32) Alaei, R.; Vaddi, Y.; Boyd, R. W. Dynamic coherent perfect absorption in nonlinear metasurfaces. *Opt. Lett.* **2020**, *45*, 6414–6417.
- (33) Bruno, V.; et al. Negative Refraction in Time-Varying Strongly Coupled Plasmonic-Antenna–Epsilon-Near-Zero Systems. *Phys. Rev. Lett.* **2020**, *124*, No. 043902.
- (34) Paul, J.; Miscuglio, M.; Gui, Y.; Sorger, V.; Wahlstrand, J. Two-beam coupling by a hot electron nonlinearity. *Opt. Lett.* **2021**, *46*, 428.
- (35) Bruno, V.; Vezzoli, S.; DeVault, C.; Roger, T.; Ferrera, M.; Boltasseva, A.; Shalaev, V. M.; Faccio, D. Dynamical control of broadband coherent absorption in ENZ films. *Micromachines* **2020**, *11*, 110.
- (36) Bruno, V.; Vezzoli, S.; DeVault, C.; Carnemolla, E.; Ferrera, M.; Boltasseva, A.; Shalaev, V. M.; Faccio, D.; Clerici, M. Broad frequency shift of parametric processes in epsilon-near-zero time-varying media. *Appl. Sci.* **2020**, *10*, 1318.
- (37) Lapshina, N.; Noskov, R.; Kivshar, Y. S. Nonlinear nano-antenna with self-tunable scattering pattern. *JETP Lett.* **2013**, *96*, 759–764.
- (38) Smirnova, D.; Kivshar, Y. S. Multipolar nonlinear nanophotonics. *Optica* **2016**, *3*, 1241–1255.
- (39) Camacho-Morales, R.; Rahmani, M.; Kruk, S.; Wang, L.; Xu, L.; Smirnova, D. A.; Solntsev, A. S.; Miroshnichenko, A.; Tan, H. H.; Karouta, F.; et al. Nonlinear generation of vector beams from AlGaAs nanoantennas. *Nano Lett.* **2016**, *16*, 7191–7197.
- (40) Smirnova, D.; Kruk, S.; Leykam, D.; Melik-Gaykazyan, E.; Choi, D.-Y.; Kivshar, Y. Third-Harmonic Generation in Photonic Topological Metasurfaces. *Phys. Rev. Lett.* **2019**, *123*, 103901.
- (41) Smirnova, D.; Smirnov, A. I.; Kivshar, Y. S. Multipolar second-harmonic generation by Mie-resonant dielectric nanoparticles. *Phys. Rev. A: At., Mol., Opt. Phys.* **2018**, *97*, No. 013807.
- (42) Carletti, L.; Koshelev, K.; De Angelis, C.; Kivshar, Y. Giant Nonlinear Response at the Nanoscale Driven by Bound States in the Continuum. *Phys. Rev. Lett.* **2018**, *121*, No. 033903.
- (43) Boyd, R. W. *Nonlinear Optics*; Academic Press, 2019.
- (44) Alaei, R.; Rockstuhl, C.; Fernandez-Corbaton, I. An electromagnetic multipole expansion beyond the long-wavelength approximation. *Opt. Commun.* **2018**, *407*, 17–21.
- (45) Bohren, C. F.; Huffman, D. R. *Absorption and Scattering of Light by Small Particles*; John Wiley & Sons, 2008.
- (46) Tribelsky, M. I.; Luk'yanchuk, B. S. Anomalous light scattering by small particles. *Phys. Rev. Lett.* **2006**, *97*, 263902.
- (47) Tribelskii, M. Resonant scattering of light by small particles. *Sov. Phys. JETP* **1984**, *59*, 534–536.
- (48) Alaei, R.; Albooyeh, M.; Rockstuhl, C. Theory of metasurface based perfect absorbers. *J. Phys. D: Appl. Phys.* **2017**, *50*, 503002.
- (49) Evlyukhin, A. B.; Novikov, S. M.; Zywiets, U.; Eriksen, R. L.; Reinhardt, C.; Bozhevolnyi, S. I.; Chichkov, B. N. Demonstration of magnetic dipole resonances of dielectric nanospheres in the visible region. *Nano Lett.* **2012**, *12*, 3749–3755.
- (50) Kuznetsov, A. I.; Miroshnichenko, A. E.; Fu, Y. H.; Zhang, J.; Luk'yanchuk, B. Magnetic light. *Sci. Rep.* **2012**, *2*, 492.
- (51) Tretyakov, S. *Analytical Modeling in Applied Electromagnetics*; Artech House, 2003.
- (52) Alaei, R.; Albooyeh, M.; Rahimzadegan, A.; Mirmoosa, M. S.; Kivshar, Y. S.; Rockstuhl, C. All-dielectric reciprocal bianisotropic nanoparticles. *Phys. Rev. B: Condens. Matter Mater. Phys.* **2015**, *92*, 245130.
- (53) Asadchy, V. S.; Díaz-Rubio, A.; Tretyakov, S. A. Bianisotropic metasurfaces: physics and applications. *Nanophotonics* **2018**, *7*, 1069–1094.
- (54) Newton, R. G. Optical theorem and beyond. *Am. J. Phys.* **1976**, *44*, 639–642.
- (55) Harrington, R. F. *Time-Harmonic Electromagnetic Fields*; IEEE, 2001; pp 168–171.
- (56) Sounas, D. L.; Alù, A. Extinction symmetry for reciprocal objects and its implications on cloaking and scattering manipulation. *Opt. Lett.* **2014**, *39*, 4053–4056.
- (57) Asadchy, V. S.; Mirmoosa, M. S.; Díaz-Rubio, A.; Fan, S.; Tretyakov, S. A. Tutorial on Electromagnetic Nonreciprocity and Its Origins. *Proc. IEEE* **2020**, *108*, 1684–1727.
- (58) Liu, W.; Kivshar, Y. S. Generalized Kerker effects in nanophotonics and meta-optics. *Opt. Express* **2018**, *26*, 13085–13105.

(59) Asadchy, V. S.; Ra'di, Y.; Vehmas, J.; Tretyakov, S. A. Functional Metamirrors Using Bianisotropic Elements. *Phys. Rev. Lett.* **2015**, *114*, No. 095503.

(60) Ra'di, Y.; Simovski, C.; Tretyakov, S. Thin perfect absorbers for electromagnetic waves: theory, design, and realizations. *Phys. Rev. Appl.* **2015**, *3*, No. 037001.

(61) Ra'di, Y.; Sounas, D. L.; Alù, A. Metagratings: Beyond the limits of graded metasurfaces for wave front control. *Phys. Rev. Lett.* **2017**, *119*, No. 067404.

(62) Slobzhanyuk, A.; Mousavi, S. H.; Ni, X.; Smirnova, D.; Kivshar, Y. S.; Khanikaev, A. B. Three-dimensional all-dielectric photonic topological insulator. *Nat. Photonics* **2017**, *11*, 130–136.